2D Ti_3C_2 MXene AND TiO_2/Ti_3C_2 HETEROSTRUCTURE: SYNTHESIS, CHARACTERIZATION, AND APPLICATION IN WASTEWATER TREATMENT VIA METHYLENE BLUE ADSORPTION

A DISSERTATION

SUBMITTED IN PARTIAL FULFILLMENT OF THE REQUIREMENTS FOR THE AWARD OF THE DEGREE

OF

MASTERS OF SCIENCE
IN
PHYSICS

Submitted by:
SATYA PRAKASH MOHANTY
23/MSCPHY/66
&
BAIBHAV BIBHUTI
23/MSCPHY/12

Under the supervision of
DR. DESHRAJ MEENA

DEPARTMENT OF APPLIED PHYSICS

DELHI TECHNOLOGICAL UNIVERSITY

(Formerly Delhi College of Engineering)

Bawana Road, Delhi – 110042

JUNE, 2025

DEPARTMENT OF APPLIED PHYSICS

DELHI TECHNOLOGICAL UNIVERSITY

(Formerly Delhi College of Engineering)

Bawana road, Delhi – 110042

CANDIDATE'S DECLARATION

We, SATYA PRAKASH MOHANTY, Roll No(s). 23/MSCPHY/66 and BAIBHAV BIBHUTI, 23/MSCPHY/12 students of M.Sc. Physics hereby declares that the project Dissertation titled "2D Ti_3C_2 MXene and TiO_2/Ti_3C_2 heterostructure: Synthesis, Characterization, and application in wastewater treatment via methylene blue adsorption" which is submitted by us to the Department of Applied Physics, Delhi Technological University, Delhi in partial fulfilment of the requirement for the award of the degree of Master of Science is original and not copied from any source without proper citation. This work has not previously formed the basis for the award of any Degree, Diploma Associateship, Fellowship or other similar title or recognition.

Place: Delhi

Satya Prakash Mohanty

Date: 09/06/2025

Baibhav Bibhuti

This is to certify that the student has incorporated all the corrections suggested by the examiners in the thesis and that the statement made by the candidate is correct to the best of our knowledge.

Dr. Deshraj Meena

(Assistant Professor)

DEPARTMENT OF APPLIED PHYSICS
DELHI TECHNOLOGICAL UNIVERSITY
(Formerly Delhi College of Engineering)
Bawana Road, Delhi-110042

CERTIFICATE

I hereby certify that the Project Dissertation titled "2D Ti_3C_2 MXene and TiO_2/Ti_3C_2 heterostructure: Synthesis, Characterization, and application in wastewater treatment via methylene blue adsorption" which is submitted by SATYA PRAKASH MOHANTY, Roll No.(s) 23/MSCPHY/66 and BAIBHAV BIBHUTI, 23/MSCPHY/12, Department of Applied Physics, Delhi Technological University, Delhi in partial fulfilment of the requirement for the award of the degree of Master of Science, is a record of the project work carried out by the students under my supervision. To the best of my knowledge this work has not been submitted in part or full for any Degree or Diploma to this University or elsewhere.

Place: Delhi
Date: 09/06/2025

DR. DESHRAJ MEENA
SUPERVISOR

ACKNOWLEDGEMENT

We would like to express our deepest sincere gratitude to our supervisor, Dr. Deshraj Meena, Assistant Professor, Department of Applied Physics, Delhi Technological University for giving us the opportunity to work under her guidance and for constant inspiration and incessant support throughout the project. We take this opportunity to express our indebtedness to our supervisor for her enthusiastic help, her expertise, brilliant ideas, valuable suggestions, and constant encouragement. We are grateful to acknowledge the constant help and convenience at every step of our project by all the lab members (Ph.D. scholars), Dept. of Applied Physics. Lately, we are thankful to our families and friends for their love, care, and support who patiently extended all sorts of help for accomplishing this task.

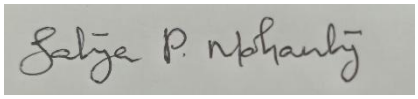

SATYA PRAKASH MOHANTY
(23/MSCPHY/66)

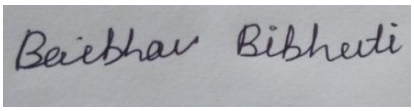

BAIBHAV BIBHUTI
(23/MSCPHY/12)

ABSTRACT

The escalating discharge of toxic, non-biodegradable dyes from industrial activities necessitates advanced remediation strategies. This study synthesizes two-dimensional $Ti_3C_2T_x$ MXene via hydrothermal etching of Ti_3AlC_2 MAX phase using $NaBF_4$/HCl, followed by delamination, and constructs a TiO_2/Ti_3C_2 heterostructure through NaOH/H_2O_2 treatment to evaluate their methylene blue (MB) adsorption efficacy. Structural characterization reveals successful Al-layer removal in MXene, evidenced by XRD peak shifts from 9.5° to 6.39° and FESEM/TEM-confirmed multilayered nanosheets. The MXene exhibits a high specific surface area, mesoporosity, and negative zeta potential of -31.8 mV, enabling 99.42% MB removal within 90 minutes via electrostatic interactions. In contrast, the TiO_2/Ti_3C_2 heterostructure, despite a larger surface area and 3D safflower-like TiO_2 morphology, shows reduced adsorption of 66.4%, due to diminished surface charges (-16.9 mV). XPS confirms terminal -O/-OH/-Cl groups in MXene, while BET analysis underscores pore structure advantages for rapid dye uptake. The heterostructure's inferior performance highlights MXene's superior standalone efficacy. This work underscores hydrothermally synthesized $Ti_3C_2T_x$ MXene as a potent, scalable adsorbent for water purification, with future potential in hybrid systems and compares its structural properties and dye adsorbing capacities with TiO_2/Ti_3C_2 heterostructure and explains why the hydrothermally synthesized pristine $Ti_3C_2T_x$ MXene is better towards synthetic dye removal than the sophisticated nanohybrids and heterostructures.

CONTENT

LIST OF FIGURES

LIST OF TABLES

LIST OF SYMBOLS AND ABBREVIATIONS

h-MXene	Hydrothermally synthesized MXene
2-D	2-dimensional
DI water	Deionised water
UV-Vis	Ultraviolet-Visible
MAX	$M_{n+1}X_nT_x$
MB	Methylene Blue
XPS	X-ray Photoelectron Spectroscopy
BET	Brunauer-Emmett-Teller
XRD	X-ray Diffraction
FESEM	Field Emission Scanning Electron Microscope
TEM	Transmission Electron Microscope
SAED	Selected Area Electron Diffraction

CHAPTER 1

INTRODUCTION AND OBJECTIVES

1.1 INTRODUCTION

MXenes represent a revolutionary class of two-dimensional (2D) inorganic materials composed of transition metal carbides, nitrides, and carbonitrides[1]. Discovered in 2011 at Drexel University, these materials bridge the gap between ceramics and nanomaterials, offering a unique combination of metallic conductivity, mechanical robustness, and tunable surface chemistry[2]. Derived from MAX phases-ternary layered precursors with the formula $M_{n+1}X_nT_x$ (where M = transition metal, A = group 13/14 element, and X = carbon/nitrogen)- MXenes are synthesized by selectively etching the 'Al' layer, leaving atomically thin sheets terminated with functional groups (-OH, -O, -F)[2]. Their versatility has propelled research across energy storage, environmental remediation, biomedicine, and electronics, positioning them as transformative materials for sustainable technologies. The discovery of MXenes emerged from collaborative work by Yury Gogotsi and Michel Barsoum, who sought to exfoliate MAX phases. The first MXene, $Ti_3C_2T_x$, was produced by hydrofluoric acid (HF) etching of Ti_3AlC_2, yielding a layered "accordion-like" structure[3]. This breakthrough unlocked a new paradigm in materials science, with over 30 compositions (e.g., V_2CT_x, $Mo_2TiC_2T_x$) now synthesized.

Recent advancements include scalable synthesis techniques, such as hydrothermal and solvothermal methods, which refine particle size and surface chemistry[4]. For instance, hydrothermal treatment at 150°C produces nitrogen-doped $Ti_3C_2T_x$ quantum dots with tunable optical properties. Despite progress, challenges persist in achieving uniform defect-free layers and large-scale production[5]. MXenes exhibit a hexagonal lattice structure with the general formula $M_{n+1}X_nT_x$ where surface terminations (T_x) dictate reactivity whose key properties include electrical conductivity which is upto 20,000 S/cm, rivaling graphene, due to delocalized d-electrons in transition metals, mechanical Strength: Young's modulus exceeding 300 GPa, enabling integration into flexible electronics, hydrophilicity: Water dispersibility facilitated by -OH/-O groups, critical for biomedical and environmental applications, thermal Stability: Retain structure up to 1,000°C in inert environments, with thermal conductivity reaching 55.8 W/(m·K) for $Ti_3C_2T_x$[6].

The surface chemistry of MXenes is highly tunable. Functionalization with polymers (e.g., polyethyleneimine) or metals (e.g., Au nanoparticles) enhances properties like catalytic activity or ion intercalation. For example, $Ti_3C_2T_x$ functionalized with polyvinyl alcohol (PVA) forms flexible membranes for water purification, while nitrogen doping improves lithium-ion storage capacity in batteries[7].

MXenes excel in energy storage due to their pseudocapacitive behavior and high surface area. As supercapacitors, $Ti_3C_2T_x$ films achieve volumetric capacitances of 1,500 F/cm³, outperforming carbon-based materials[8]. Their layered structure enables rapid ion diffusion, with 92% capacitance retention after 10,000 cycles. As batteries, Nb_2CT_x anodes deliver 420 m Ah/g in lithium-ion batteries, while MXene-coated separators mitigate polysulfide shuttling in lithium-sulphur systems[9]. Doping with transition metals (e.g., Mo) enhances theoretical capacities to 745 m Ah/g. For the generation of solar Energy, MXene/TiO_2 hybrids drive hydrogen evolution at rates of 12 mmol/g/h under UV-vis light, leveraging their high photothermal conversion efficiency[9]. In the field of environmental remediation, MXenes' hydrophilicity and surface charge make them ideal for water treatment. For heavy metal removal, $Ti_3C_2T_x$ adsorbs Pb^{2+} at 1,200 mg/g, while composites with g-C_3N_4 degrade 98% of methylene blue under visible light[10]. For desalination purpose lamellar $Ti_3C_2T_x$ membranes reject 97% of divalent ions (e.g., Mg^{2+}) via size exclusion and electrostatic repulsion. Janus membranes combining $Ti_3C_2T_x$ with WS_2 exhibit threefold higher water permeance than conventional materials. As sensors, $Ti_3C_2T_x$ detects NH_3 at 1 ppm through resistivity changes, with potential for air quality monitoring. MXenes' biocompatibility and optical properties drive biomedical advances such as drug delivery, pH-responsive $Ti_3C_2T_x$ -PVA hydrogels enable controlled release of doxorubicin, reducing off-target toxicity[11].

For photothermal Therapy, $Ti_3C_2T_x$ converts near-infrared light to heat, achieving 90% tumor ablation in vivo. Gold-MXene hybrids enhance contrast in computed tomography and photoacoustic imaging[12].

MXene composites inhibit bacterial growth (e.g., E. coli) through physical disruption and reactive oxygen species generation which make them a useful candidate for antibacterial coatings[13]. Due to their excellent conductivity and flexibility, MXenes, it enable next-generation electronics and Optoelectronic devices. As EMI Shielding $Ti_3C_2T_x$ films (2.5 μm) attenuate 92 dB of electromagnetic interference, surpassing metals[14]. As flexible Sensors: MXene/PDMS composites exhibit a gauge factor of 500, ideal for wearable strain sensors. Blade-coated $Ti_3C_2T_x$ films act as transparent electrodes, achieve 83% transmittance with 19,325 S/cm conductivity, rivaling indium tin oxide (ITO) in solar cells and touchscreens[15].

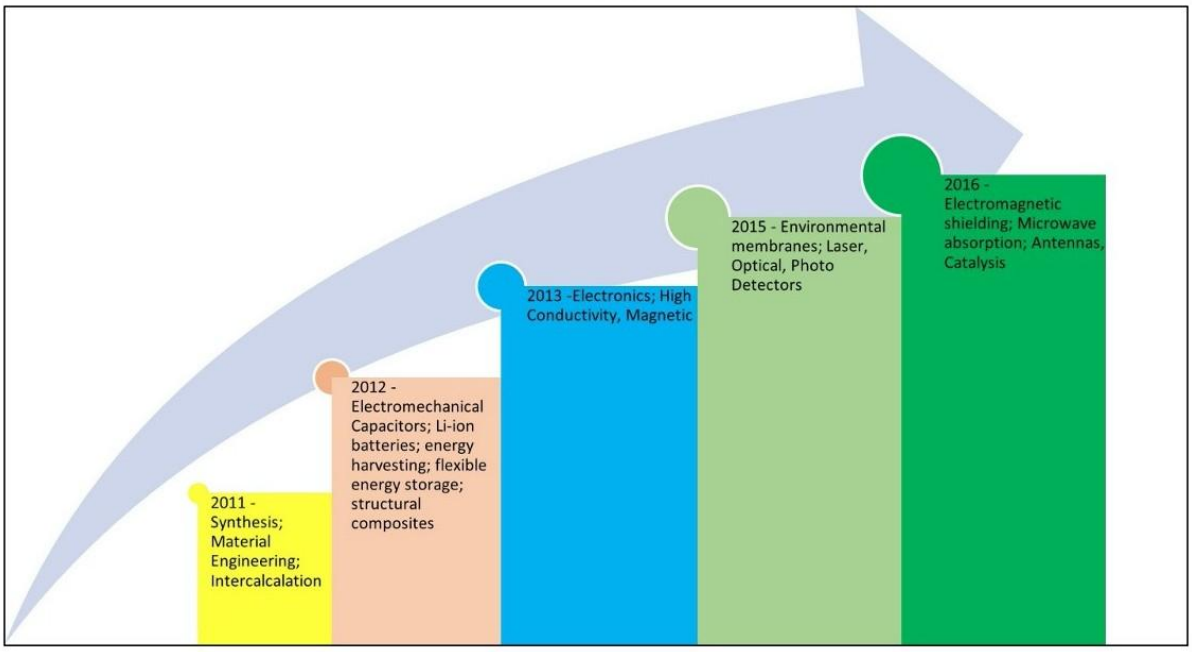

Fig. 1 $Ti_3C_2T_x$ MXene application history

MXenes are synthesized through diverse methods that balance safety, scalability, and material performance. These methods broadly fall into top-down etching, bottom-up synthesis, and hybrid approaches, each offering unique advantages and challenges[15]. The most common route involves selectively removing the "Al" layer (e.g., Al, Ga) from MAX phases ($M_{n+1}AX_n$) using Hydrofluoric Acid (HF) Etching: Direct etching of MAX phases (e.g., Ti_3AlC_2) with concentrated HF yields MXenes like $Ti_3C_2T_x$.[16] While effective, HF's toxicity and corrosivity necessitate stringent safety protocols, including fume hoods and protective gear. Safer alternatives use HCl/LiF mixtures to generate HF in situ, reducing hazards while enabling lithium intercalation for delamination[17]. Another method is molten Salt Etching, by employing salts like $ZnCl_2$ or $SnCl_2$ at high temperatures (550–873°C) avoids HF entirely. This method introduces tunable surface terminations (e.g., Cl, S) and produces stable MXenes, though it requires energy-intensive conditions.

Electrochemical Etching is another similar method where by utilizing electrolytes like HBF_4, this HF-free method selectively dissolves the 'Al' layer via anodic oxidation[18]. It scales efficiently and yields MXenes with larger lateral dimensions, ideal for supercapacitors.

There are also bottom-up synthesis methods of bypassing MAX phases, constructing MXenes atom-by-atom. One such method is Chemical Vapor Deposition (CVD), which involves reacting metal halides (e.g., $TiCl_4$) with carbon/nitrogen sources (e.g., CH_4, N_2) on substrates produces high-purity MXenes. CVD enables vertical alignment (e.g., Ti_2CCl_2 "carpets") and novel morphologies like vesicles, enhancing applications in catalysis and energy storage.

Hydrothermal/Solvothermal synthesis involves aqueous or solvent-based reactions under high pressure/temperature (e.g., NaOH etching of Mo_2Ga_2C) yield MXene quantum dots (QDs) for bioimaging, though reaction times are prolonged[19]. Recent research follows some hybrid and advanced methods like mechanochemical Pretreatment: ball milling MAX phases before etching increases interlayer spacing, improving etching efficiency and electrochemical performance[20]. Template-assisted assembly: 3D-printed templates guide MXene aerogel formation via cation-induced gelation, creating architectures for high-capacity energy storage[21].

With surge in rapid industrialization across the globe, amount of air and water pollution also has been increased exponentially. The textile, leather, and paper industries are major contributors to global water pollution, releasing billions of liters of dye-contaminated wastewater annually[22]. Synthetic dyes, such as azo, anthraquinone, and triarylmethane compounds, are chemically stable, non-biodegradable, and often toxic. Approximately 10–15% of dyes used in industrial processes are discharged untreated into water bodies, contaminating aquatic ecosystems and threatening biodiversity[23]. These dyes block sunlight penetration, impairing photosynthesis in algae and aquatic plants, which disrupts oxygen levels and destabilizes aquatic food chains. Additionally, dye effluents elevate biochemical oxygen demand (BOD) and chemical oxygen demand (COD), depleting dissolved oxygen and causing hypoxia, which suffocates marine life. Heavy metals like lead, chromium, and cadmium, frequently present in industrial

effluents, exacerbate toxicity, leading to bioaccumulation in fish and eventual entry into the human food chain[24]. Chronic exposure to these pollutants is linked to cancers, organ failure, and neurological disorders. Soil irrigated with contaminated water suffers reduced fertility, altered microbial ecosystems, and inhibited crop growth, undermining agricultural sustainability[25].

Conventional remediation methods, such as activated carbon adsorption, chemical precipitation, and biological treatments, face limitations. Activated carbon is costly and inefficient for low-concentration dyes, while chemical methods generate toxic sludge[26]. Biological processes struggle with dye recalcitrance, and advanced oxidation techniques are energy-intensive. MXenes—emerging two-dimensional materials composed of transition metal carbides, nitrides, or carbonitrides—offer a groundbreaking solution. Synthesized by selectively etching the "Al" layer from MAX phases (e.g., Ti_3AlC_2), MXenes like $Ti_3C_2T_x$ exhibit a layered structure, high surface area (~1,500 m^2/g), and tunable surface terminations (-OH, -O, -F), making them exceptional adsorbents[27].

MXenes excel in dye removal due to their negatively charged surfaces, which electrostatically attract cationic dyes (e.g., methylene blue, malachite green) and form hydrogen bonds with organic pollutant[28]. For instance, $Ti_3C_2T_x$ MXene achieved 99.1% removal of malachite green within 150 minutes, while MXene-Co_3O_4 composites demonstrated a 136.24 mg/g adsorption capacity for methylene blue, surpassing conventional adsorbents[29]. Functionalization with polymers

(e.g., chitosan) or nanoparticles (e.g., ZnO) enhances selectivity and efficiency. MXene/ZnO hybrids removed 97% of Pb^{2+} and As^{3-} via synergistic effects, showcasing versatility in addressing mixed contaminants[30]. The dye removal efficiencies of different adsorbent [31]materials have been noted in Table 1. MXenes also address challenges like reusability and scalability. Regeneration via thermal treatment or solvent washing retains more than 90% efficiency after multiple cycles[32]. Green synthesis methods, such as molten salt etching (e.g., $ZnCl_2$/KCl), avoid toxic hydrofluoric acid (HF), reducing environmental hazards. Their mechanical flexibility enables integration into membranes for continuous filtration systems[33]. For example, Fe_3O_4/Ti_3C_2 composites combine magnetic separation with high adsorption, simplifying recovery and reuse[34].

In this work, we have synthesized 2D MXene $Ti_3C_2T_x$ nanosheets using a hydrothermal route from precursor MAX phase MAX-phase Ti_3AlC_2. In the next step a unique safflower shaped TiO_2/Ti_3C_2 heterostructure with three-dimensional (3D) porous frameworks was synthesized from Ti_3C_2Tx MXene[35]. The synthesized Ti_3C_2Tx MXene and $TiO_2/Ti3C_2$ were subjected to different material characterizations, and their structural properties were investigated[36]. Further we have performed dye adsorption[37] test on both the synthesized materials and and based on the results, a comparative analysis on their adsorbance property is done[38].

Table 1. Different materials and their dye removal efficiencies

S.no.	Material	Morphology	Dye	Dye removal efficency
1	SnO_2 / MXene	Bulk structure to form sheets where both SnO_2 & MXene are agglomerated.	MB	70% for 120 mins under direct sunlight.
2	TiO_2 / MXene	Layered of Ti_3C_2 MXene and an array of TiO_2 particles on the external MXene surface.	MO	99% for 40 mins under light irradiation.
3	TiO_2 /MXene	Spherical TiO_2 particle uniformly supported on MXene nanosheet.	MB	96.44% in UV light for 60 mins.
4	ZnO/ MXene	ZnO particle dispersed over the loose accordion-shape layered structure with smooth surface. At higher temperature ZnO micro-rods & twinned ZnO structure.	RhB	97.5% with 18 mins under UV light.
5	ZnO/ MXene	Flower like ZnO loaded on the surface of MXene in the form of rods.	MB	94.8% with 180 mins in visible light.
6	ZnO/ RGO	RGO sheet are exfolliated and intact with ZnO providing a composite material	CR	98% for 90 mins with (PH-10) alkaline.
7	TiO_2/RGO	TiO2 NPs	RhB	94.55% for 120 mins in light.
8	ZnO/SnO_2/ RGO	SnO_2/ZnO-core shell nanostructure RGO- nanosheet	CR	Orange-II = 99.8% reactive red = 97.02 for 120 mins under visible light.
9	SnO_2/ gC_3N_4	Condenced layer of porous gC_3N_4 covering the surface of SnO_2	RhB	99.42% for 150 mins under led-30 W.
10	Cu-ZnO/gC_3N_4	Wurzite structure bundles with hexagonal nanorods	RhB MB	98% & 99% for 40 mins under UV light.

11	TiO_2/gC_3N_4	TiO_2 nanoparticle on the surface of gcn nanosheet	Sodium diclofenac	99.99% for 120 mins with scavenger.
12	Ta (3%) -WO_3	WO3-irregularly shaped rough nano spheroid. Ta/WO_3-sharp and porous nano cubes of diff. nm. range.	MB	91% IN 120mins under 400 W power metal halide lamp.
13	Ta (3%)-TiO_2	TiO_2 NPs	RhB MB	91% &88% for 120mins under UV light.
14	WO_3/Ti_3C_2	2D-2D nanosheets	MB	92%, for 105mins

CHAPTER 2

EXPERIMENTAL

2.1 Material and Reagents

37 wt% Sodium tetraborofluorate ($NaBF_4$) provided by Vizak Chemicals. 30% HCl was bought from Green Agri Solution. Ti_3AlC_2 (MAX phase) was purchased from Aritech Chemazone pvt. Ltd. 1M NaOH solution and 30% Hydrogen Peroxide (H_2O_2) was bought from Annexe Chem pvt. Ltd. Methylene Blue (MB) provided by Jalan Dyestuff Co.

2.2 SYNTHESIS METHODS

2.2.1 Hydrothermal synthesis of $Ti_3C_2T_x$ MXene

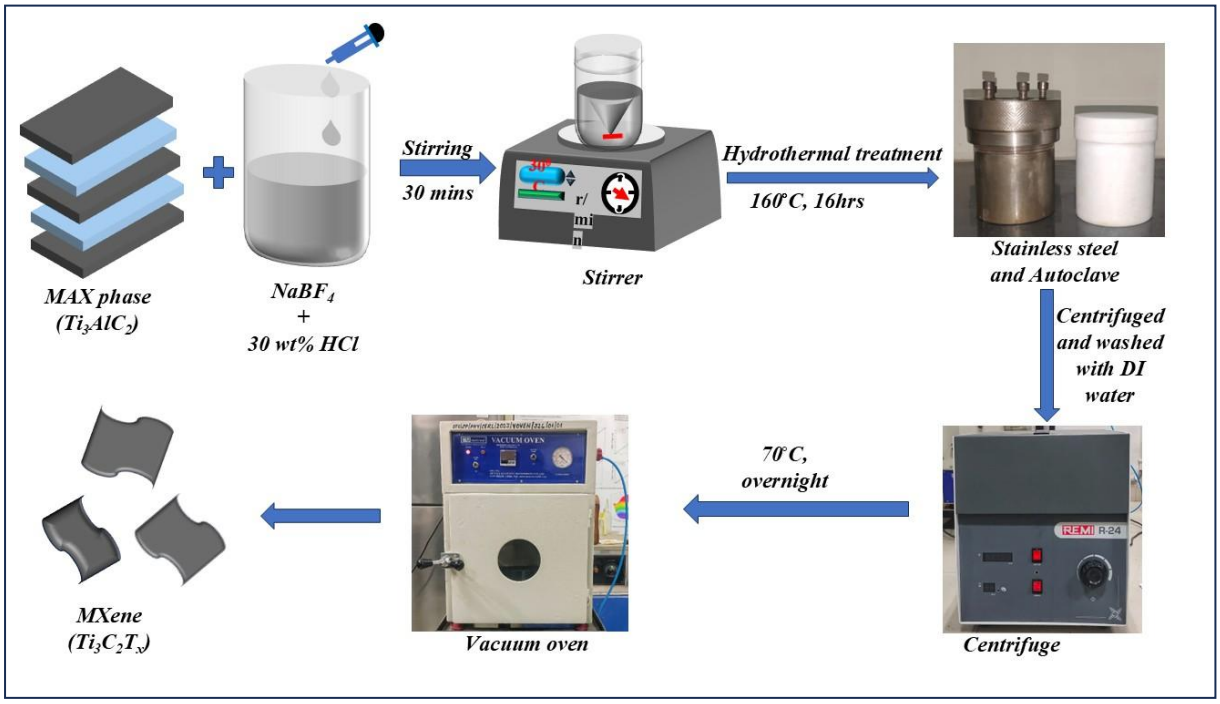

Fig. 2 Schematic representation of hydrothermal synthesis of $Ti_3C_2T_x$ MXene

The hydrothermal synthesis of h-Ti_3C_2 MXene involves a series of precise chemical steps. Sodium tetrafluoroborate ($NaBF_4$) is dissolved in 37 wt% hydrochloric acid (HCl). To this solution, titanium aluminium carbide (Ti_3AlC_2) is added and the mixture is stirred until uniform. This suspension is then transferred to a 100 mL autoclave, ensuring that it is filled to no more than 30% of its capacity, hydrothermally treated at 180 °C for a duration ranging from 8 to 32 hours[39].

2.2.2 Synthesis of TiO_2/Ti_3C_2 heterostructure

The one-step synthesis method for TiO_2/Ti_3C_2 heterostructures can be effectively performed using a hydrothermal approach. In this process, $Ti_3C_2T_x$ MXene is used as both the substrate and titanium source. First, 200 mg of Ti_3C_2 powder is dispersed in deionized water to form a suspension. This suspension is then treated with 60 ml of 1 M NaOH and 4 ml of 30% H_2O_2, which is added to the mixture. The resulting solution is transferred to a Teflon-lined autoclave and subjected to hydrothermal treatment at 160 °C for 12 hours. This treatment facilitates the growth of TiO_2 directly on the Ti_3C_2 surface, forming a heterojunction that enhances photocatalytic properties. After cooling, the product can be washed and dried to obtain the $TiO_2/Ti3C_2$ heterostructure[40], [41].

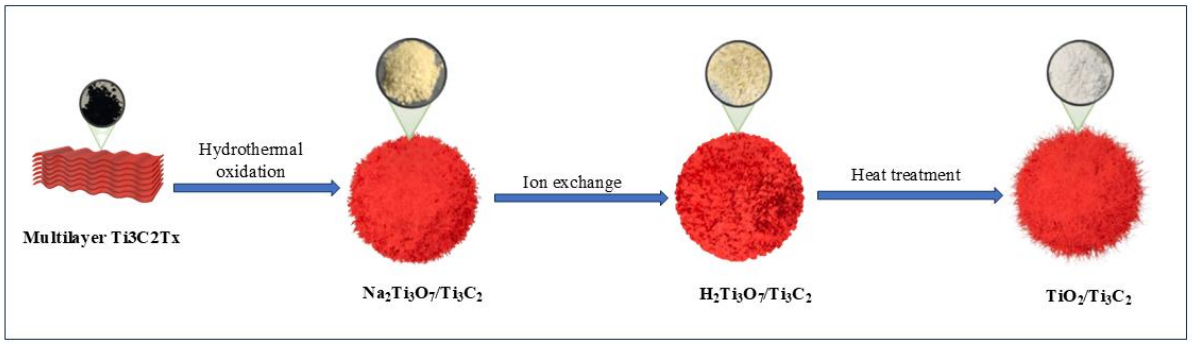

Fig. 3 Schematic representation of stepwise synthesis of TiO_2/Ti_3C_2

2.3 Characterization Techniques

The crystal structure of the synthesized $Ti_3C_2T_x$ MXene and TiO_2/Ti_3C_2 heterostructure was studied using X-ray Diffraction (XRD, Rigaku MNCF 030) with Cu Kα1 and Cu Kα2 radiation. Surface morphology was investigated using a field emission scanning electron microscope (FESEM, FEI NOVA NANOSEM-450) with energy dispersive x-ray spectrometer (EDX) mounted. TEM, HRTEM and SAED pattern study reveals the detailed structure, fringe pattern, grain boundary and atomic arrangement using a transmission electron microscope (TEM, JOEL/JEM-F200). Brunauer-Emmett-Teller (BET, BELSORP max II) study was carried out to find out the specific surface area by N2 adsorption-desorption curve. The surface elemental analysis and binding energies were determined by X-ray photoelectron spectrometer (XPS, Kratos Analytical MNCF 026) with Al Kα radiation. Zeta potential for both the samples was evaluated using Malvern Panalytical zetasizer.

2.4 Dye adsorption test

To test the adsorption capacity of $Ti_3C_2T_x$ and TiO_2/Ti_3C_2, dye adsorption test was conducted, for which MB was taken as the main probing dye. A stock solution was prepared whose concentration is taken to be 31 µm (1mg in 100 ml of deionized water). The adsorbent amount was taken to be 25 mg. In order to avoid any photocatalytic effect, the whole setup was kept inside dark environment. The rate of MB dye removal efficency was evaluated using the following formula

$$R\ (\%) = [(A_o - A_t)/A_o] \times 100$$

CHAPTER 3

RESULTS AND DISCUSSIONS

3.2.1. XRD

Fig. 4 is the XRD pattern which reveals the crystallinity and phase structure of the synthesized $Ti_3C_2T_x$ MXene and and TiO_2/Ti_3C_2 heterostructure. The precursor Ti_3AlC_2 (MAX phase) shows characteristic peaks at 9.5°, 19.1° and 39.1°[42] which corresponds to the (002), (004) and (104) planes (JCPDS 52-0875). When, it is subjected to hydrothermal etching, the Al layer gets removed. As a result the interplanar distance increases.

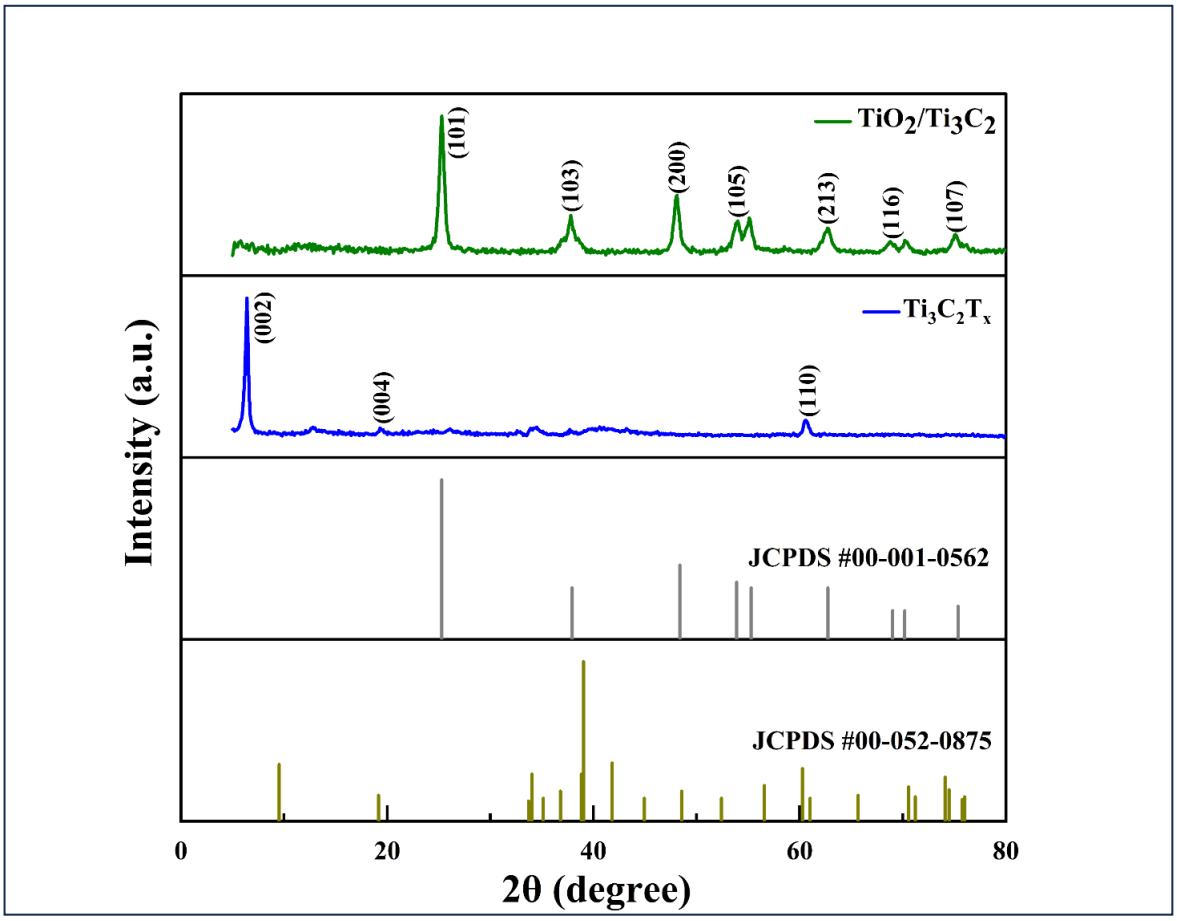

Fig. 4 XRD pattern of $Ti_3C_2T_x$ and and TiO_2/Ti_3C_2

This can be observed from the XRD pattern that the most intense peak at 39.1° correspond to (104) plane of Ti3AlC2 has been completely vanished and the peaks at 19.1° and 60.2° which correspond to (004) and (110) planes have been diminished and the peak at 9.5° has been shifted to 6.39°[43]. This confirms the formation of MXene from the MAX phase. Further when the $Ti_3C_2T_x$ MXene was subjected to hydrothermal oxidation, followed by ion exchange and heat treatment, a drastic change in the XRD pattern was observed[44]. New peaks were observed at 25.3°, 38.1°, 48.4°, 53.9°, 62.7°, 69°, 75.4° which correspond to (101), (103), (200), (105), (213), (116), (107) diffraction planes of anatase TiO_2 (JCPDS 01-0562)[45]. The d-spacing was calculated to be 13.83Å and 3.52Å for $Ti_3C_2T_x$ MXene and TiO_2/Ti_3C_2 heterostructure respectively. Further using debye-scherrer's formula, crystallite size of both the samples were determined to be 18.15nm and 20.37 nm[46], [47].

3.2.2 FESEM with EDX mapping

The surface morphology of the synthesized $Ti_3C_2T_x$ MXene and TiO_2/Ti_3C_2 heterostructure were examined using a field-emission scanning electron microscope (FEI, NOVA NANOSEM-450). It can be clearly observed from Fig. 5(a, b) that the randomly arranged MAX phase have been successfully transformed into multilayered MXene nanosheets, which further confirms the etching of Al layers. Some small granules can be observed in the FESEM image, which are due to incomplete transformation of MAX phase to $Ti_3C_2T_x$[48], [49]. This could be achieved by increasing the hydrothermal etching time but by doing so chances of agglomeration would be high. Fig. 5(c, d) are the FESEM images of TiO_2/Ti_3C_2 heterostructure, where

3D safflowers of TiO_2 has been emerged out of the 2D MXene which well resembles with previously reported literature[40], [41].

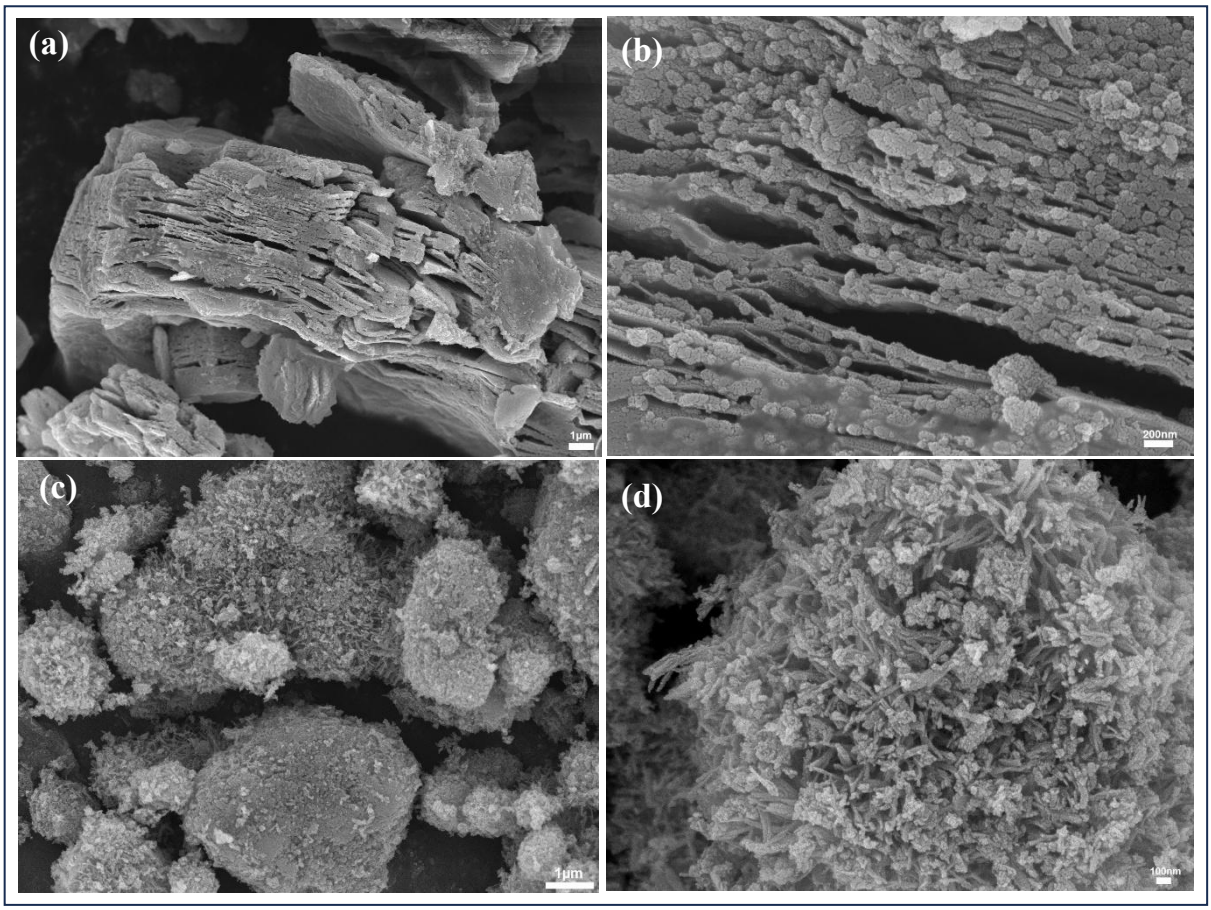

Fig. 5 FESEM images of (a,b) $Ti_3C_2T_x$ and (c,d) TiO_2/Ti_3C_2

Electron dispersive x-ray spectrometry (EDX) is used to determine the chemical environment and elemental distribution in the synthesized material which can be seen in fig. 6. Table 2 depicts the elements present in Ti3C2Tx and their atomic %, where (C: O:Cl:Ti::14.5:12.1:5.7:65.8) are present and there is no tress of Al, which suggests the etching of Al layer from the Ti3AlC2 MAX phase. Likewise, in the case of TiO2/Ti3C2 heterostructure, there is only (C: O:Ti ::17.8:44.9:37.4) are present. Surface termination groups like oxides and halides are absent, which makes it less anionic species than $Ti_3C_2T_x$.

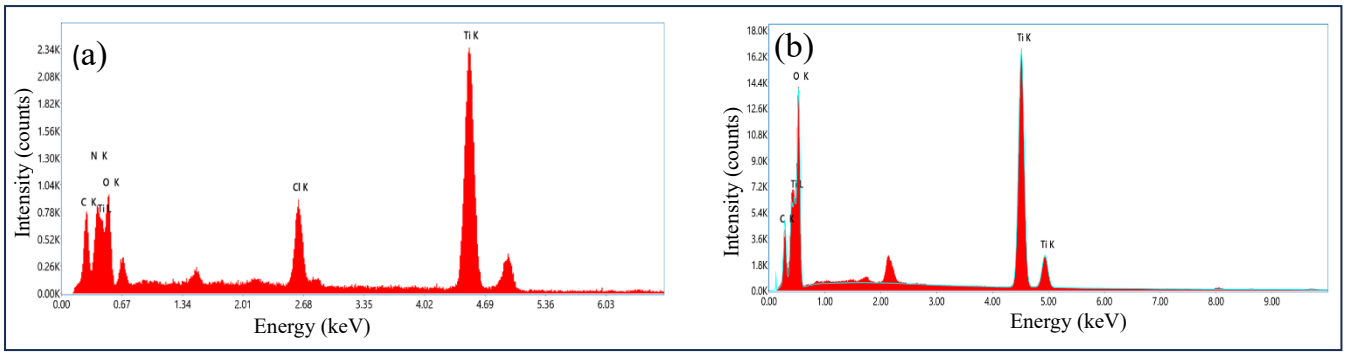

Fig. 6 EDX spectrum of (a) $Ti_3C_2T_x$ (b) TiO_2/Ti_3C_2

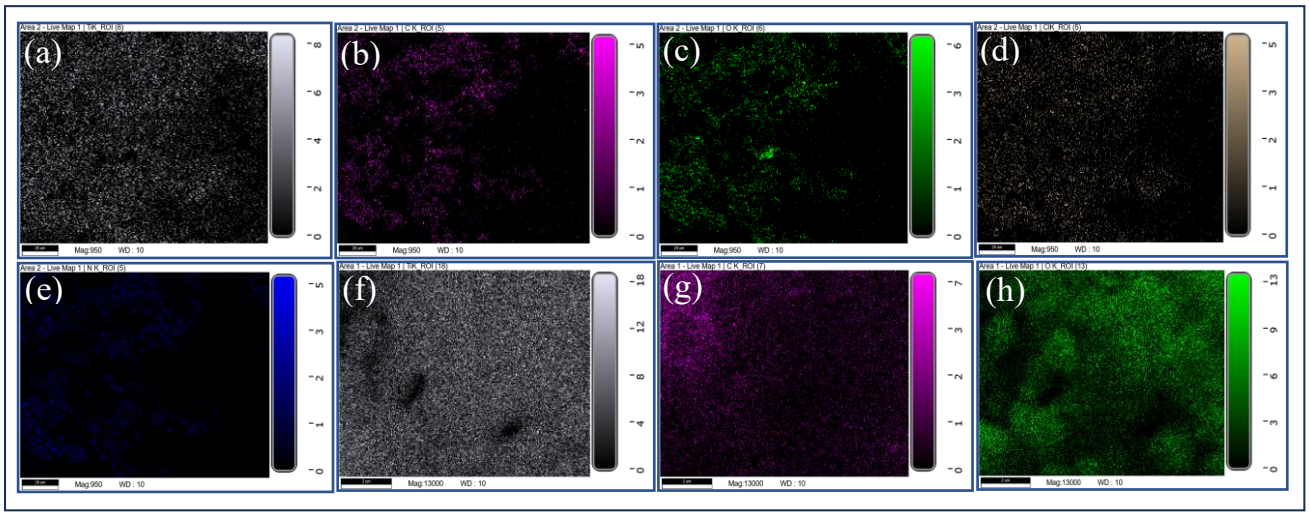

Fig. 7 EDX elemental mapping of (a-e) $Ti_3C_2T_x$ and (f-h) TiO_2/Ti_3C_2

Table 2. Elemental composition of (a) $Ti_3C_2T_x$ and (b) TiO_2/Ti_3C_2

(a)

Element	Weight %	Atomic %
C K	14.1	32.1
N K	3.1	6.0
O K	11.7	20.1
Cl K	5.7	4.4
Ti K	65.4	37.4

(b)

Element	Weight %	Atomic %
C K	17.8	29.2
O K	44.9	55.4
Ti K	37.4	15.4

3.2.3 TEM

The detailed microstructural view of the synthesized $Ti_3C_2T_x$ MXene and TiO_2/Ti_3C_2 heterostructure was viewed under transmission Electron Microscope (TEM) which shows the layered structure of $Ti_3C_2T_x$. High-resolution transmission electron microscopy (HRTEM) reveals lattice fringes of 0.31 nm, corresponding to the (100) planes of $Ti_3C_2T_x$, and confirms the presence of defect-free, ultrathin sheets. Selected-area electron diffraction (SAED) patterns exhibit hexagonal symmetry, validating the crystalline structure of MXene[50].

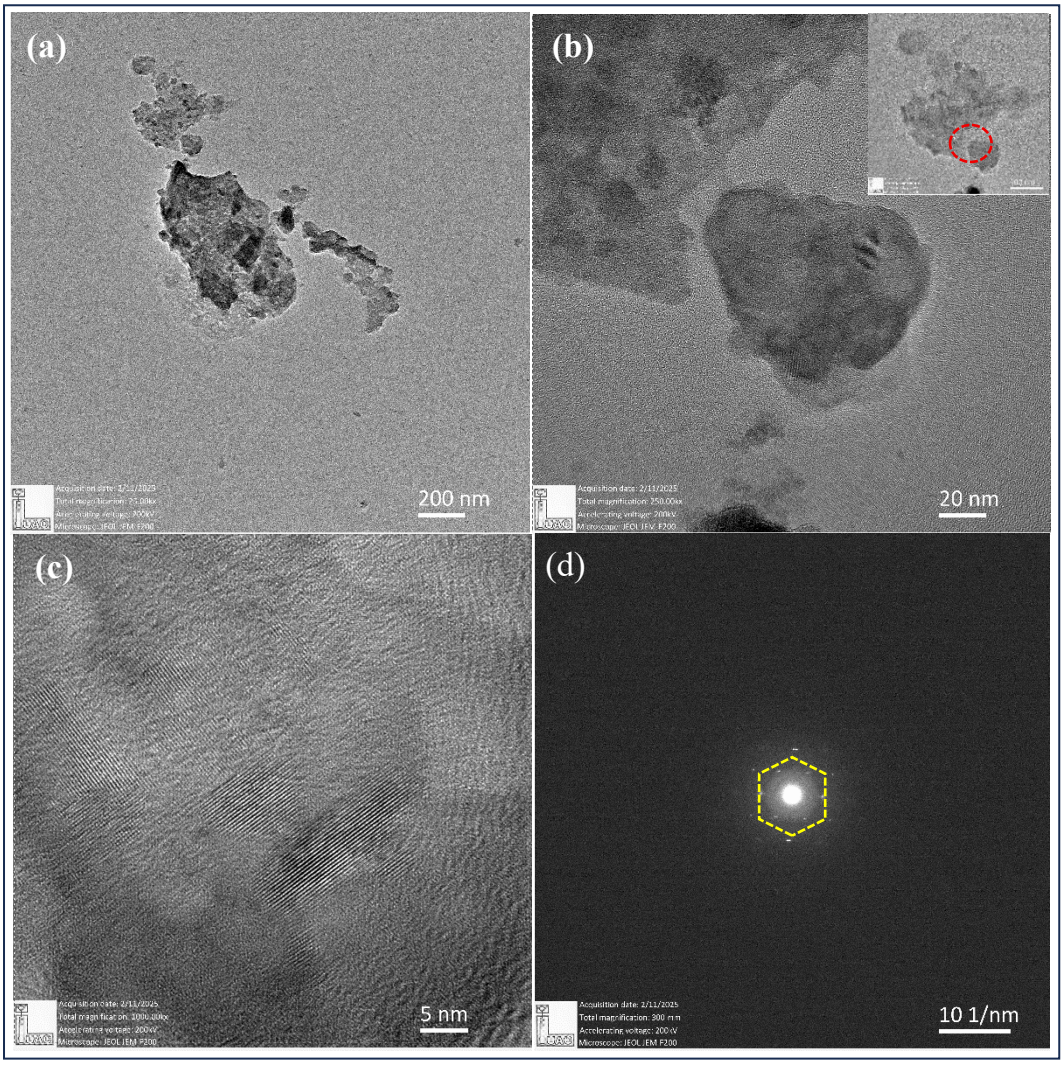

Fig. 8 (a, b) TEM, (c) HRTEM, (d) SAED pattern images of $Ti_3C_2T_x$

For TiO_2/Ti_3C_2 heterostructures, hydrothermal oxidation methods facilitate the growth of TiO_2 nanosheets on MXene surfaces. Cross-sectional TEM imaging shows interlayer spacing reductions from ~1.1 nm (pristine MXene) to ~0.35 nm post-oxidation, indicative of TiO_2 integration. HRTEM highlights epitaxial alignment between anatase TiO_2 (0.35 nm lattice spacing for (101) planes) and Ti_3C_2, with SAED confirming composite diffraction rings from both phases. Elemental mapping via EDS underscores uniform Ti, C, and O distribution, while HAADF-STEM imaging visualizes surface functional groups and interfacial coherence[40], [41].

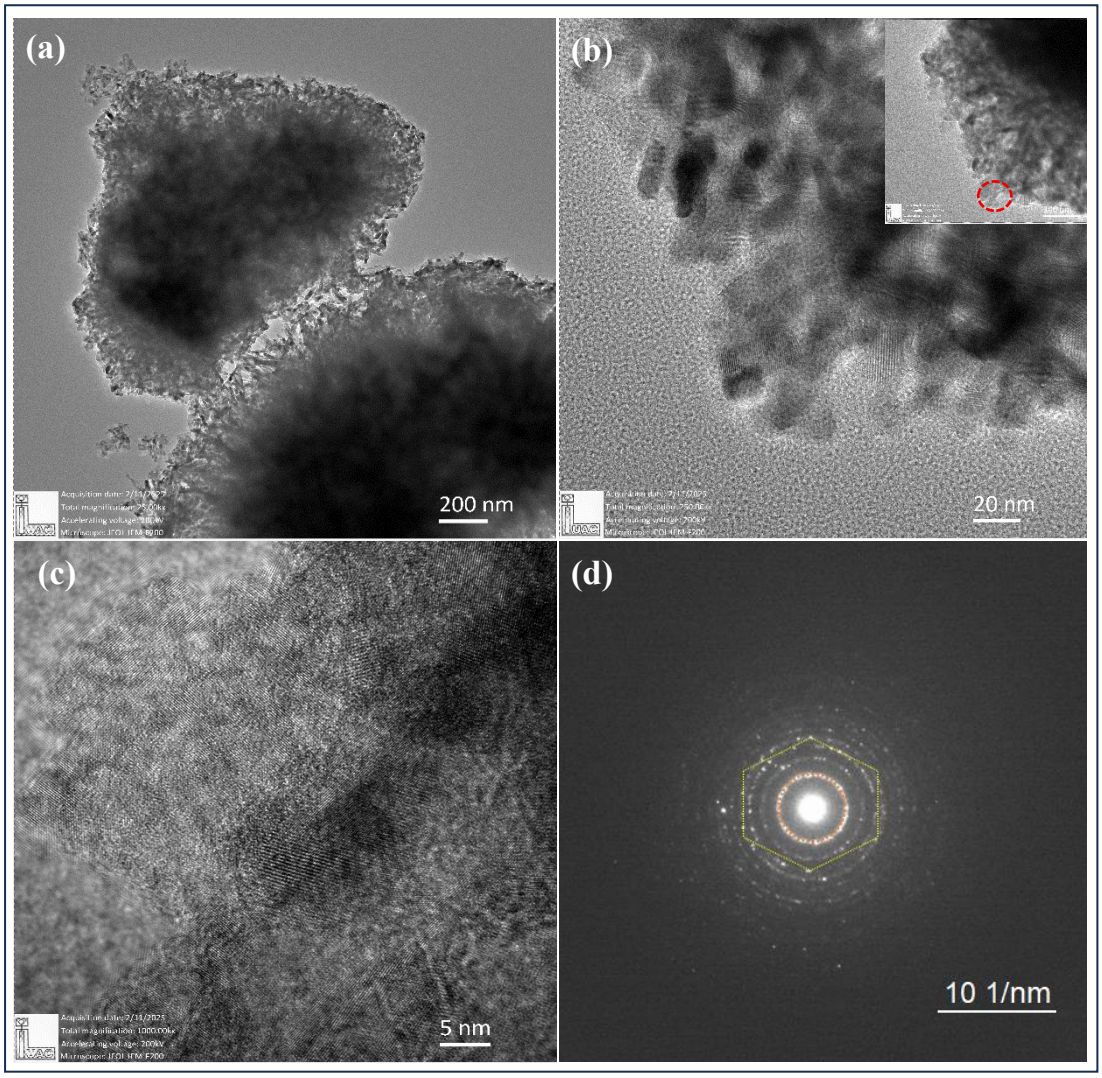

Fig. 9 (a, b) TEM, (c) HRTEM, (d) SAED pattern images of TiO2/Ti3C2

3.2.4 XPS

X-ray photoelectron spectroscopy (XPS) is pivotal in elucidating the surface chemistry of $Ti_3C_2T_x$ MXene. In $Ti_3C_2T_x$ MXene, survey spectra reveals the elemental composition which contains O 1s, Ti 2p, C 1s, F 1s, Cl 2p with at.% 37.7, 17.92, 32.47, 6.88, 5.03 and peak binding energy position at at 532 eV, 459.97 eV, 286.47 eV, 685.98 eV, 200.35 eV. High-resolution Ti 2p scan reveal distinct bonding states: Ti–C (456 eV), Ti–O (457 eV), Ti–F (458 eV), and TiO_2 (459 eV), indicating surface terminations (-O, -OH, -F, -Cl) and partial oxidation[50], [51].

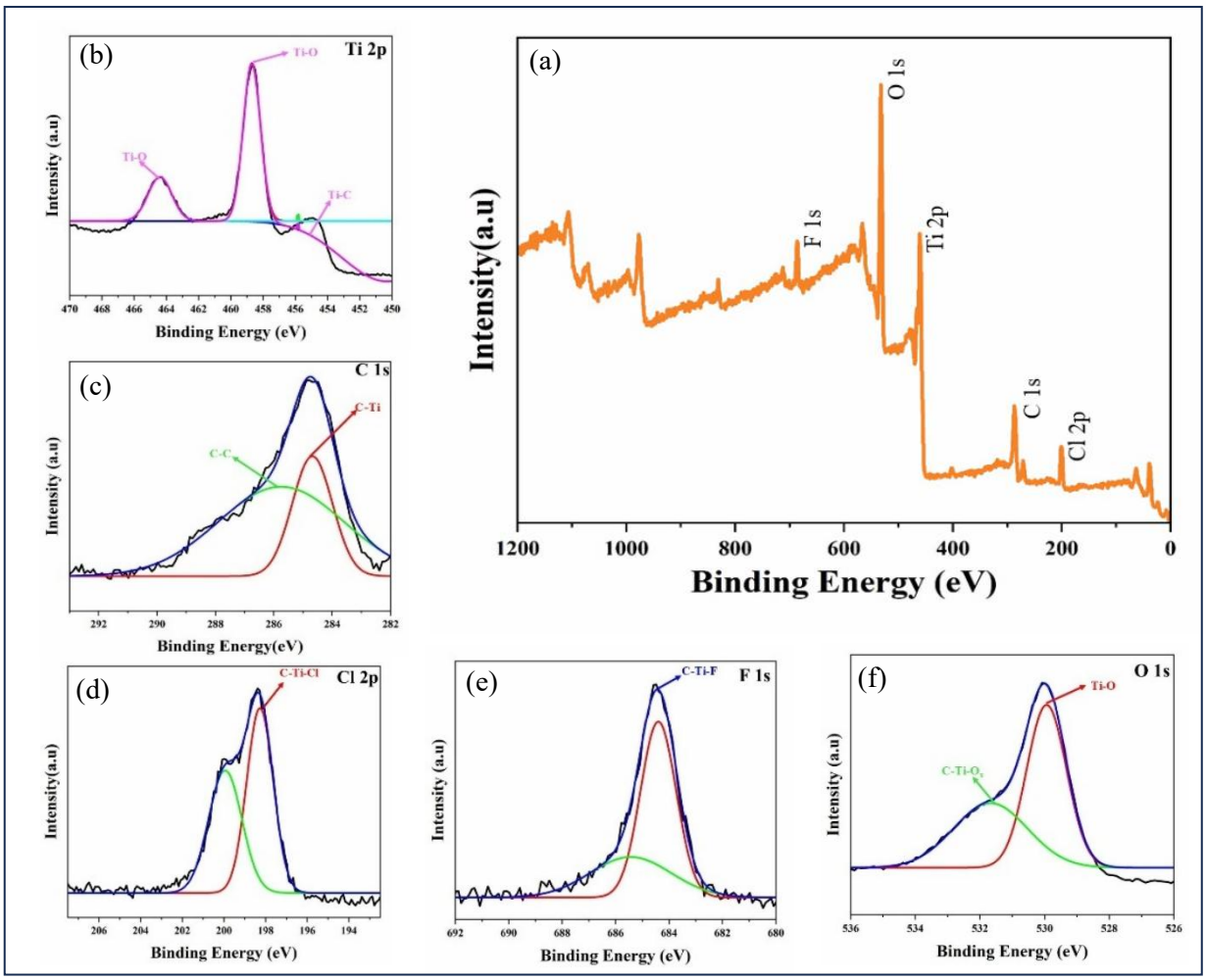

Fig. 10 (a) XPS survey spectra, (b-f) high resolution scan of Ti 2p, C 1s, O 1s, F 1s, Cl 2p of $Ti_3C_2T_x$

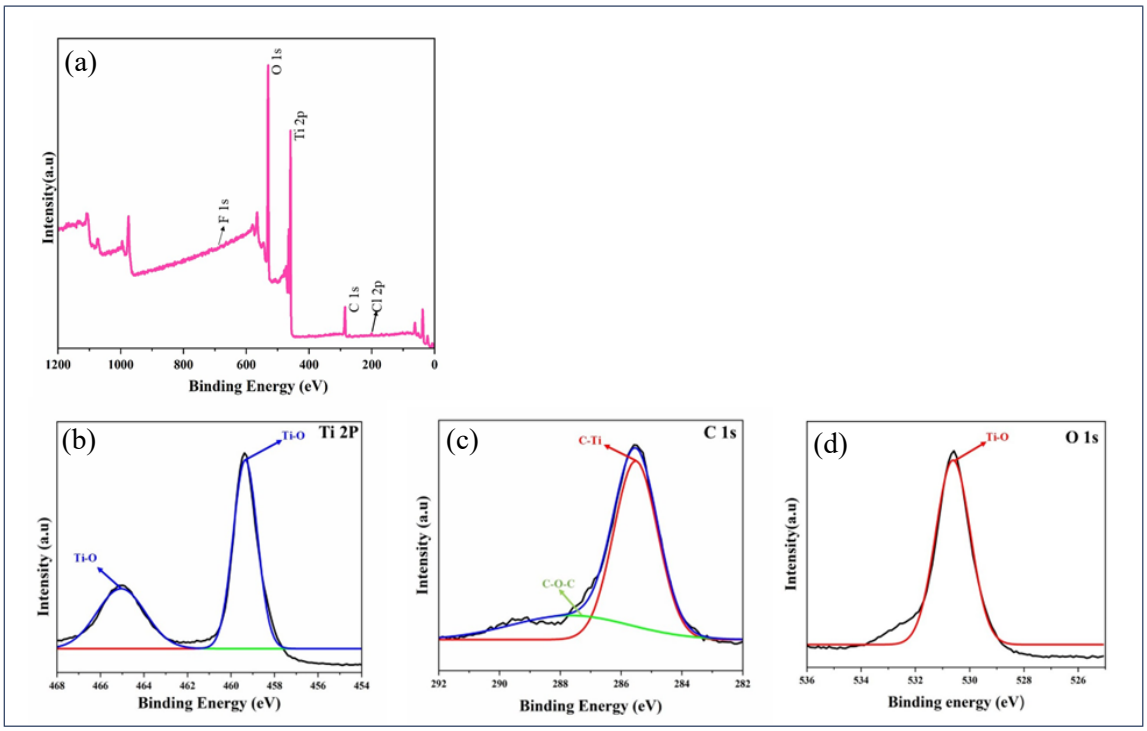

Fig. 11 (a) XPS survey spectra, (b-d) high resolution scan of Ti 2p, C 1s, O 1s of TiO_2/Ti_3C_2

The C 1s spectrum features Ti–C (282 eV) and adventitious carbon (284.8 eV), while O 1s peaks correspond to Ti–O (530 eV), Ti–OH (531.5 eV), and adsorbed H_2O (533 eV). F 1s spectra (686 eV) confirm Ti–F bonds. For TiO_2/Ti_3C_2 heterostructures, XPS highlights TiO_2 formation with Ti content (29.2 at.%) (Ti^{4+} at 459 eV) and reduced F content (0.15 at.%), and Cl content (0.99 at.%) suggesting almost absence of surface groups, enhancing its stability. The O 1s spectrum shifts toward lattice oxygen (530 eV), with residual Ti–OH and H_2O. Hierarchical structures, such as 1D TiO_2 nanowires on 2D Ti_3C_2, mitigate layer stacking and oxidation, confirmed by cross-sectional analysis. Surface chemistry reveals increasing O (44.6 at.%) and reducing C (24.5 at.%), while maintaining Ti–C integrity[40], [41].

3.2.5 BET

BET method is critical for evaluating the specific surface area (SSA) and porosity of $Ti_3C_2T_x$ MXene and TiO_2/Ti_3C_2 heterostructure. For $Ti_3C_2T_x$, BET analysis reveals the SSA value is determined to be 153.63 m^2/g, with pore volumes of 0.27 cm^3/g and average pore diameters of 16.8Å[52]. Nitrogen adsorption-desorption isotherms for $Ti_3C_2T_x$ often conform to Type IV (IUPAC classification) isotherm with H3 hysteresis, indicative of slit-shaped mesopores formed by aggregated nanosheets. The Barrett-Joyner-Halenda (BJH) pore size distribution confirms narrow mesopore ranges, enhancing dye adsorption. For TiO_2/Ti_3C_2 heterostructures, BET surface area is determined to be 181.22 m^2/g, influenced by TiO_2 nanoparticle size and distribution[53]. The increased surface area of TiO_2/Ti_3C_2 may attributed to the 3D flower like structure of TiO2 but the incorporation of TiO_2 introduces new mesopores with pore volumes of 0.31 cm^3/g and average pore diameters of 18Å which partially block MXene pores[54], [55]. So, further zeta potential test was conducted to determine the adsorbent action over MB.

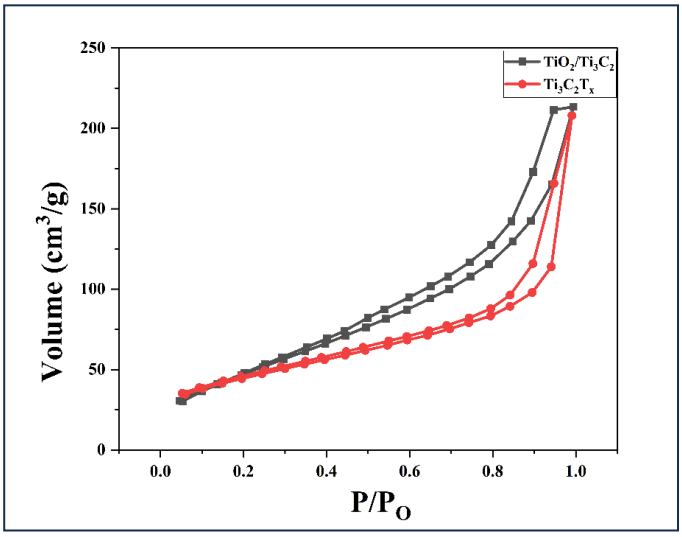

Fig. 12 N_2 adsorption-desorption isotherm for $Ti_3C_2T_x$ and andTiO_2/Ti_3C_2

3.2.6 ZETA POTENTIAL

$Ti_3C_2T_x$ MXene being an anionic species exhibits a strongly negative surface charge before adsorption, with zeta potential value -31.8 mV in neutral PH conditions. This negativity is due to the presence of deprotonated surface groups ($-O^-$, $-OH^-$) and chlorine terminations ($-Cl^-$). Following methylene blue (MB) adsorption, the zeta potential shifted to -16 mV, this lowering in negative zeta potential reflects electrostatic neutralization as cationic MB^+ ions bind to the MXene surface[51]. This interaction reduces charge density, confirming electrostatic attraction as the primary adsorption mechanism. For TiO_2/Ti_3C_2 heterostructures, the initial zeta potential is less negative (-16.9 mV) compared to pristine $Ti_3C_2T_x$ due to absence of ($-Cl^-$). Post-MB adsorption, the zeta potential further decreases to -11 mV. Comparing the zeta potential values, one can conclude that pristine $Ti_3C_2T_x$ shows better adsorbance properties towards MB removal from waste water, which also makes adsorption an efficient way of MB removal from water rather than photocatalytic dye degradation, which demands more sophisticated materials.

3.2.7 DYE REMOVAL EFFICIENCY

- The MB removal efficiencies of $Ti_3C_2T_x$ MXene and TiO_2/Ti_3C_2 heterostructure were examined by conducting dye adsorption test. Real time absorbance vs concentration plots were plotted for both $Ti_3C_2T_x$ MXene and TiO_2/Ti_3C_2 heterostructure. The result shows $Ti_3C_2T_x$ removes 92.6% of MB from the stock solution within just 15 minutes and the optimum removal efficiency is 99.42% after 90 minutes, which also reflect in decolorization of the stock solution. Whereas, in the case of TiO_2/Ti_3C_2, no significant decolorization is observed and the MB removal efficiency was calculated to be 81.4% only in 90 minutes.

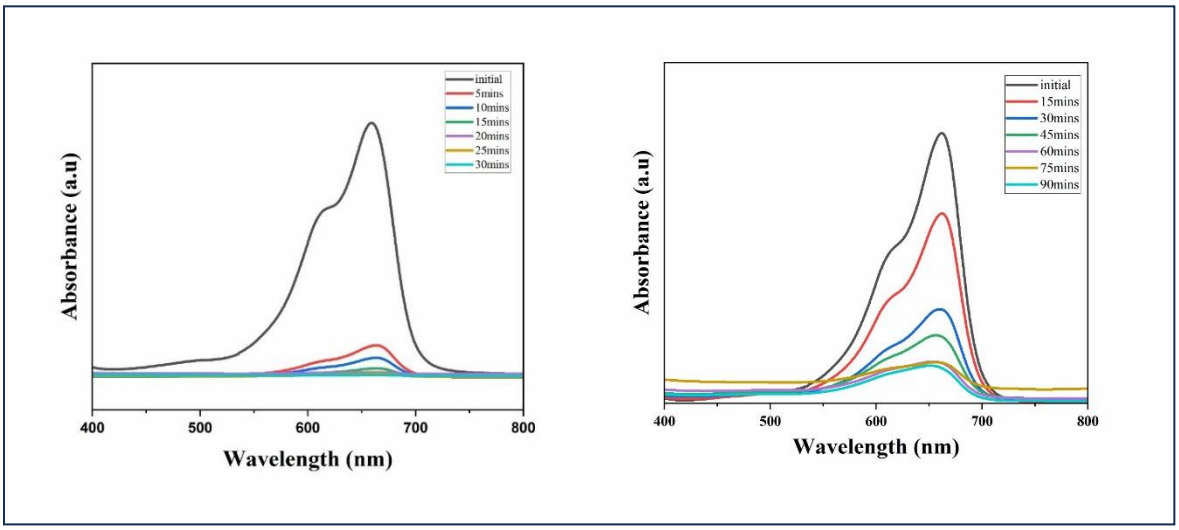

Fig. 14 Real time UV-Vis absorbance plot for (a) $Ti_3C_2T_x$ (b) TiO_2/ Ti_3C_2

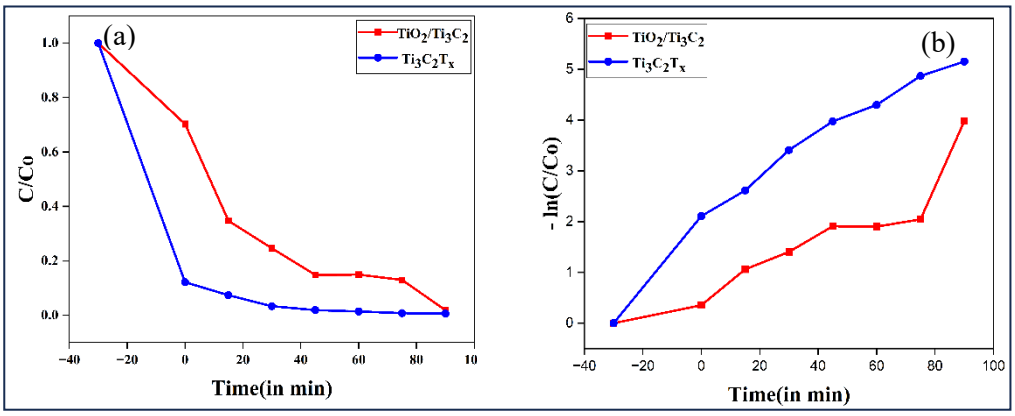

Fig. 15 (a) MB concentration with time (b) Mb removal efficiency with time

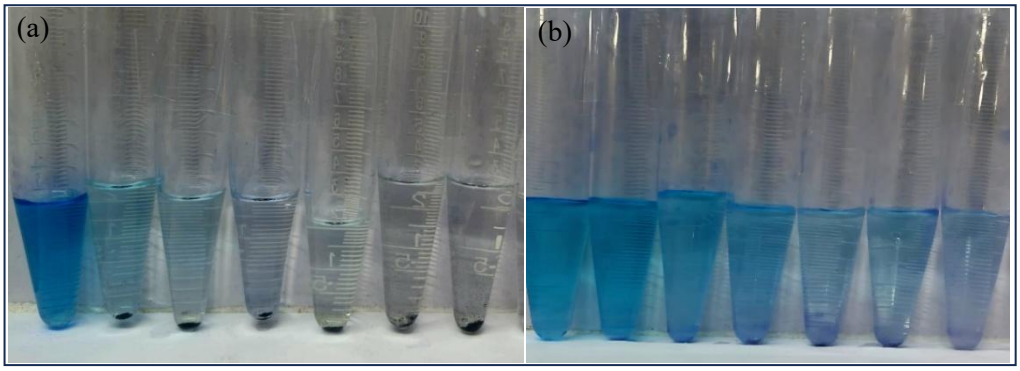

Fig. 16 Decolorization of MB solution using (a) $Ti_3C_2T_x$ (b) TiO_2/ Ti_3C_2

CHAPTER - 4

CONCLUSIONS AND FUTURE SCOPE

4.1. Conclusion

The synthesized $Ti_3C_2T_x$ MXene demonstrated exceptional methylene blue (MB) adsorption efficiency, achieving 99.42% removal within 90 minutes, attributed to its high specific surface area (153.63 m^2/g), negatively charged surface (-31.8 mV zeta potential), and layered structure facilitating electrostatic interactions with cationic dyes. Characterization via XRD confirmed the successful etching of the Al layer from the Ti_3AlC_2 MAX phase, evidenced by the shift of the (002) peak from 9.5° to 6.39° and the disappearance of the (104) peak at 39.1°. FESEM and TEM revealed the transformation of the MAX phase into multilayered MXene nanosheets, while BET analysis highlighted the material's mesoporous nature, crucial for rapid dye uptake. In contrast, the TiO_2/Ti_3C_2 heterostructure exhibited limited adsorption (64.6%), likely due to reduced surface terminations and altered charge distribution, as indicated by zeta potential measurements shifting from -16.9 mV to -11 mV post-adsorption. However, the heterostructure's 3D safflower-like morphology, observed in FESEM, and the presence of anatase TiO_2 (confirmed by XRD peaks at 25.3° and 48.4°) suggest untapped potential in dye adsorption.

4.2. Future Scope

Despite their promise, challenges like oxidative instability in humid environments and high production costs persist. Future research focuses on fluoride-free synthesis, surface group optimization, and pilot-scale applications. MXenes bridge material science and environmental engineering, offering a sustainable pathway to mitigate dye pollution. By leveraging their unique properties, MXenes herald a cleaner future for global water resources, demonstrating unparalleled potential in eco-friendly wastewater treatment.

REFERENCES

[1] D. M. Saju, R. Sapna, U. Deka, and K. Hareesh, “MXene material for supercapacitor applications: A comprehensive review on properties, synthesis and machine learning for supercapacitance performance prediction,” Aug. 15, 2025, *Elsevier B.V.* doi: 10.1016/j.jpowsour.2025.237302.

[2] A. Hamzehlouy and M. Soroush, “MXene-based catalysts: A review,” Jun. 01, 2024, *Academic Press*. doi: 10.1016/j.mtcata.2024.100054.

[3] S. Wang, Y. Liu, Y. Liu, and W. Hu, “Effect of HF etching on titanium carbide (Ti3C2Tx) microstructure and its capacitive properties,” *Chemical Engineering Journal*, vol. 452, Jan. 2023, doi: 10.1016/j.cej.2022.139512.

[4] Y. Liu *et al.*, “Efficient mechanical exfoliation of MXene nanosheets,” *Chemical Engineering Journal*, vol. 468, Jul. 2023, doi: 10.1016/j.cej.2023.143439.

[5] L. Liu, E. Raymundo-Piñero, P. L. Taberna, and P. Simon, “Electrochemical characterization of Ti3C2Tx MXene prepared via a molten salt etching route in an acetonitrile-based electrolyte,” *Electrochem commun*, vol. 148, Mar. 2023, doi: 10.1016/j.elecom.2023.107453.

[6] L. Liu *et al.*, “In Situ Synthesis of MXene with Tunable Morphology by Electrochemical Etching of MAX Phase Prepared in Molten Salt,” *Adv Energy Mater*, vol. 13, no. 7, Feb. 2023, doi: 10.1002/aenm.202203805.

[7] H. Shao *et al.*, “Synthesis of MAX Phase Nanofibers and Nanoflakes and the Resulting MXenes,” *Advanced Science*, vol. 10, no. 1, Jan. 2023, doi: 10.1002/advs.202205509.

[8] S. A. Sergiienko *et al.*, “Composite MAX phase/MXene/Ni electrodes with a porous 3D structure for hydrogen evolution and energy storage application,” *RSC Adv*, vol. 14, no. 5, pp. 3052–3069, Jan. 2024, doi: 10.1039/d3ra07335a.

[9] A. S. Zeraati, S. Mirkhani, P. Sun, M. Naguib, P. V Braun, and U. Sundararaj, “Supplementary Information for Improved Synthesis of Ti3C2Tx MXene Resulting in Exceptional Electrical Conductivity, High Synthesis Yield, and Enhanced Capacitance,” 2021.

[10] A. Vijayaprabhakaran and M. Kathiresan, “Fluorine-free synthesized tantalum carbide (Ta2C Mxene) as an efficient electrocatalyst for water reduction and nitro compound reduction,” *Mater Adv*, vol. 4, no. 16, pp. 3593–3602, Jul. 2023, doi: 10.1039/d3ma00223c.

[11] S. Iravani *et al.*, “Advancements in MXenes and mechanochemistry: exploring new horizons and future applications,” Sep. 16, 2024, *Royal Society of Chemistry*. doi: 10.1039/d4ma00775a.

[12] S. Iravani *et al.*, “Advancements in MXenes and mechanochemistry: exploring new horizons and future applications,” Sep. 16, 2024, *Royal Society of Chemistry*. doi: 10.1039/d4ma00775a.

[13] T. Guo *et al.*, “Rational Design of Ti3C2Tx MXene Inks for Conductive, Transparent Films,” *ACS Nano*, vol. 17, no. 4, pp. 3737–3749, Feb. 2023, doi: 10.1021/acsnano.2c11180.

[14] Y. Gogotsi and B. Anasori, “The Rise of MXenes,” Aug. 27, 2019, *American Chemical Society*. doi: 10.1021/acsnano.9b06394.

[15] B. Ahmed, A. El Ghazaly, and J. Rosen, “i-MXenes for Energy Storage and Catalysis,” Nov. 01, 2020, *Wiley-VCH Verlag*. doi: 10.1002/adfm.202000894.

[16] M. Dadashi Firouzjaei, M. Karimiziarani, H. Moradkhani, M. Elliott, and B. Anasori, “MXenes: The two-dimensional influencers,” Mar. 01, 2022, *Elsevier Ltd*. doi: 10.1016/j.mtadv.2021.100202.

[17] M. Pogorielov, K. Smyrnova, S. Kyrylenko, O. Gogotsi, V. Zahorodna, and A. Pogrebnjak, “Mxenes—a new class of two-dimensional materials: Structure, properties and potential applications,” *Nanomaterials*, vol. 11, no. 12, Dec. 2021, doi: 10.3390/nano11123412.

[18] M. Mim *et al.*, “MXene: A Roadmap to Sustainable Energy Management, Synthesis Routes, Stabilization, and Economic Assessment,” *ACS Omega*, Jul. 2024, doi: 10.1021/acsomega.4c04849.

[19] U. U. Rahman *et al.*, “molecules MXenes as Emerging Materials: Synthesis, Properties, and Applications,” 2022, doi: 10.3390/10.3390/molecules27154909.

[20] H. Naaz, F. P. Malik, A. Mahmood, and A. Irfan, “Investigation of 2D Nb3C2-Based MXenes as the Anode Material for LIBs: A Theoretical Study,” *ACS Omega*, Feb. 2025, doi: 10.1021/acsomega.4c01473.

[21] S. Kumar *et al.*, “Effect of Ti3C2T: XMXenes etched at elevated temperatures using concentrated acid on binder-free supercapacitors,” *RSC Adv*, vol. 10, no. 68, pp. 41837–41845, Nov. 2020, doi: 10.1039/d0ra05376g.

[22] S. Kumar *et al.*, “Effect of Ti3C2T: XMXenes etched at elevated temperatures using concentrated acid on binder-free supercapacitors,” *RSC Adv*, vol. 10, no. 68, pp. 41837–41845, Nov. 2020, doi: 10.1039/d0ra05376g.

[23] R. M. Ronchi, J. T. Arantes, and S. F. Santos, “Synthesis, structure, properties and applications of MXenes: Current status and perspectives,” Oct. 15, 2019, *Elsevier Ltd*. doi: 10.1016/j.ceramint.2019.06.114.

[24] X. Pan *et al.*, “2D MXenes polar catalysts for multi-renewable energy harvesting applications,” *Nat Commun*, vol. 14, no. 1, Dec. 2023, doi: 10.1038/s41467-023-39791-w.

[25] C. Rong *et al.*, “Elastic properties and tensile strength of 2D Ti3C2Tx MXene monolayers,” *Nat Commun*, vol. 15, no. 1, Dec. 2024, doi: 10.1038/s41467-024-45657-6.

[26] R. Bian, S. Xiang, and D. Cai, “Fast Treatment of MXene Films with Isocyanate to Give Enhanced Stability,” *ChemNanoMat*, vol. 6, no. 1, pp. 64–67, Jan. 2020, doi: 10.1002/cnma.201900602.

[27] Z. Ahmadian, M. J. Azad, S. Mohammadi, Y. Mortazavi, and A. A. Khodadadi, “The effect of ball-milling parameters on the structures of Ti3AlC2 MAX phase and resultant Ti3C2Tx MXene,” *Journal of Ultrafine Grained and Nanostructured Materials*, vol. 55, no. 2, pp. 112–121, 2022, doi: 10.22059/jufgnsm.2022.02.03.

[28] B. C. Wyatt *et al.*, “Alkali cation stabilization of defects in 2D MXenes at ambient and elevated temperatures,” *Nat Commun*, vol. 15, no. 1, Dec. 2024, doi: 10.1038/s41467-024-50713-2.

[29] S. Bai *et al.*, “Recent advances of MXenes as electrocatalysts for hydrogen evolution reaction,” Dec. 01, 2021, *Nature Research*. doi: 10.1038/s41699-021-00259-4.

[30] W. Ding *et al.*, “Highly sensitive and reversible MXene-based micro quartz tuning fork gas sensors with tunable selectivity,” *NPJ 2D Mater Appl*, vol. 8, no. 1, Dec. 2024, doi: 10.1038/s41699-024-00452-1.

[31] C. E. Shuck, K. Ventura-Martinez, A. Goad, S. Uzun, M. Shekhirev, and Y. Gogotsi, “Safe Synthesis of MAX and MXene: Guidelines to Reduce Risk during Synthesis,” *ACS Chemical Health and Safety*, vol. 28, no. 5, pp. 326–338, Sep. 2021, doi: 10.1021/acs.chas.1c00051.

[32] F. M. Oliveira *et al.*, “Synthesis of tubular MXenes with carbon fiber template and use as anodes in lithium-ion batteries,” *Commun Mater*, vol. 6, no. 1, Dec. 2025, doi: 10.1038/s43246-025-00786-3.

[33] Y. Guo *et al.*, “Synthesis of Mo2C MXene with high electrochemical performance by alkali hydrothermal etching,” *Journal of Advanced Ceramics*, vol. 12, no. 10, pp. 1889–1901, Oct. 2023, doi: 10.26599/JAC.2023.9220795.

[34] K. C. Chan *et al.*, “The fabrication of Ti3C2 and Ti3CN MXenes by electrochemical etching,” Apr. 12, 2024. doi: 10.26434/chemrxiv-2024-qf7hk.

[35] L. Verger, C. Xu, V. Natu, H. M. Cheng, W. Ren, and M. W. Barsoum, “Overview of the synthesis of MXenes and other ultrathin 2D transition metal carbides and nitrides,” Jun. 01, 2019, *Elsevier Ltd*. doi: 10.1016/j.cossms.2019.02.001.

[36] T. Yousaf, A. Areeb, M. Murtaza, A. Munir, Y. Khan, and A. Waseem, “Silane-Grafted MXene (Ti3C2TX) Membranes for Enhanced Water Purification Performance,” *ACS Omega*, vol. 7, no. 23, pp. 19502–19512, Jun. 2022, doi: 10.1021/acsomega.2c01143.

[37] S. Tian, G. Cheng, Z. Tang, F. Sha, Z. Xuan, and G. Ding, “Fabrication of two-dimensional Ti3C2Tx MXenes by ball milling pretreatment and mild etchant and their microstructure,” *Ceram Int*, vol. 46, no. 18, pp. 28949–28954, Dec. 2020, doi: 10.1016/j.ceramint.2020.08.065.

[38] N. Xue, X. Li, M. Zhang, L. Han, Y. Liu, and X. Tao, “Chemical-combined ball-milling synthesis of fluorine-free porous MXene for high-performance lithium ion batteries,” *ACS Appl Energy Mater*, vol. 3, no. 10, pp. 10234–10241, Oct. 2020, doi: 10.1021/acsaem.0c02081.

[39] C. Peng *et al.*, “A hydrothermal etching route to synthesis of 2D MXene (Ti3C2, Nb2C): Enhanced exfoliation and improved adsorption performance,” *Ceram Int*, vol. 44, no. 15, pp. 18886–18893, Oct. 2018, doi: 10.1016/j.ceramint.2018.07.124.

[40] N. My Tran, Q. Thanh Hoai Ta, and J. S. Noh, “Unusual synthesis of safflower-shaped TiO2/Ti3C2 heterostructures initiated from two-dimensional Ti3C2 MXene,” *Appl Surf Sci*, vol. 538, Feb. 2021, doi: 10.1016/j.apsusc.2020.148023.

[41] V. T. Quyen *et al.*, “Advanced synthesis of MXene-derived nanoflower-shaped TiO2@Ti3C2 heterojunction to enhance photocatalytic degradation of Rhodamine B,” *Environ Technol Innov*, vol. 21, Feb. 2021, doi: 10.1016/j.eti.2020.101286.

[42] S. Sukidpaneenid, C. Chawengkijwanich, C. Pokhum, T. Isobe, P. Opaprakasit, and P. Sreearunothai, “Multi-function adsorbent-photocatalyst MXene-TiO2 composites for removal of enrofloxacin antibiotic from water,” *J Environ Sci (China)*, vol. 124, pp. 414–428, Feb. 2023, doi: 10.1016/j.jes.2021.09.042.

[43] S. Zhang *et al.*, “photocatalytic degradation of TiO2 via incorporating Ti3C2 MXene for methylene blue removal from water,” *Catal Commun*, vol. 174, Jan. 2023, doi: 10.1016/j.catcom.2022.106594.

[44] X. Huang, M. Sun, W. Sun, Z. Li, H. Chen, and J. Zhao, “One-step hydrothermal formation of porous N-graphyne decorated TiO2/Ti3C2 composites with enhanced photocatalytic activity,” *Int J Hydrogen Energy*, vol. 55, pp. 581–591, Feb. 2024, doi: 10.1016/j.ijhydene.2023.11.203.

[45] J. Chen, H. Zheng, Y. Zhao, M. Que, W. Wang, and X. Lei, “Morphology and photocatalytic activity of TiO2/MXene composites by in-situ solvothermal method,” *Ceram Int*, vol. 46, no. 12, pp. 20088–20096, Aug. 2020, doi: 10.1016/j.ceramint.2020.05.083.

[46] D. E. Lee, S. Moru, W. K. Jo, and S. Tonda, “Dual-cocatalyst-promoted photocatalytic treatment of persistent waterborne pollutants via in situ MXene-derived TiO2/Ti3C2 hybrids with plasmonic Ag nanoparticles,” *Sep Purif Technol*, vol. 352, Jan. 2025, doi: 10.1016/j.seppur.2024.128261.

[47] S. F. Hosseini, M. S. Seyed Dorraji, and M. H. Rasoulifard, “Boosting photo-charge transfer in 3D/2D TiO2@Ti3C2 MXene/Bi2S3 Schottky/Z-scheme heterojunction for photocatalytic antibiotic degradation and H2 evolution,” *Compos B Eng*, vol. 262, Aug. 2023, doi: 10.1016/j.compositesb.2023.110820.

[48] Z. Li *et al.*, “Synthesis and thermal stability of two-dimensional carbide MXene Ti3C2,” *Materials Science and Engineering: B*, vol. 191, no. C, pp. 33–40, Jan. 2015, doi: 10.1016/j.mseb.2014.10.009.

[49] P. Srimuk *et al.*, “MXene as a novel intercalation-type pseudocapacitive cathode and anode for capacitive deionization,” *J Mater Chem A Mater*, vol. 4, no. 47, pp. 18265–18271, 2016, doi: 10.1039/c6ta07833h.

[50] S. M. El-Mas, M. A. Hassaan, G. M. El-Subruiti, A. S. Eltaweil, and A. El Nemr, “Box-Behnken design optimization of 2D Ti3C2Tx MXene nanosheets as a microwave-absorbing catalyst for methylene blue dye degradation,” *Chemical Engineering Journal*, vol. 500, Nov. 2024, doi: 10.1016/j.cej.2024.156969.

[51] N. My Tran, Q. Thanh Hoai Ta, A. Sreedhar, and J. S. Noh, “Ti3C2Tx MXene playing as a strong methylene blue adsorbent in wastewater,” *Appl Surf Sci*, vol. 537, Jan. 2021, doi: 10.1016/j.apsusc.2020.148006.

[52] C. Peng *et al.*, “A hydrothermal etching route to synthesis of 2D MXene (Ti3C2, Nb2C): Enhanced exfoliation and improved adsorption performance,” *Ceram Int*, vol. 44, no. 15, pp. 18886–18893, Oct. 2018, doi: 10.1016/j.ceramint.2018.07.124.

[53] N. My Tran, Q. Thanh Hoai Ta, and J. S. Noh, “Unusual synthesis of safflower-shaped TiO2/Ti3C2 heterostructures initiated from two-dimensional Ti3C2 MXene,” *Appl Surf Sci*, vol. 538, Feb. 2021, doi: 10.1016/j.apsusc.2020.148023.

[54] Y. Liu *et al.*, “Enhanced degradation of tetracycline by TiO2@MXene with peroxydisulfate under visible light irradiation,” *Sep Purif Technol*, vol. 343, Sep. 2024, doi: 10.1016/j.seppur.2024.127122.

[55] A. K. Fard, G. Mckay, R. Chamoun, T. Rhadfi, H. Preud’Homme, and M. A. Atieh, “Barium removal from synthetic natural and produced water using MXene as two dimensional (2-D) nanosheet adsorbent,” *Chemical Engineering Journal*, vol. 317, pp. 331–342, 2017, doi: 10.1016/j.cej.2017.02.090.

Baibhav Satya

Dissertation Report Satya_Baibhav.pdf

Delhi Technological University

Document Details

Submission ID

trn:oid:::27535:99827590

Submission Date

Jun 8, 2025, 11:37 AM GMT+5:30

Download Date

Jun 8, 2025, 11:42 AM GMT+5:30

File Name

Dissertation Report Satya_Baibhav.pdf

File Size

2.5 MB

27 Pages

4,446 Words

24,506 Characters

turnitin Page 2 of 32 - Integrity Overview Submission ID trn:oid:::27535:99827590

8% Overall Similarity

The combined total of all matches, including overlapping sources, for each database.

Filtered from the Report

- Bibliography
- Quoted Text
- Cited Text
- Small Matches (less than 8 words)

Match Groups

35 Not Cited or Quoted 8%
Matches with neither in-text citation nor quotation marks

0 Missing Quotations 0%
Matches that are still very similar to source material

0 Missing Citation 0%
Matches that have quotation marks, but no in-text citation

0 Cited and Quoted 0%
Matches with in-text citation present, but no quotation marks

Top Sources

6% Internet sources
2% Publications
5% Submitted works (Student Papers)

Integrity Flags

1 Integrity Flag for Review

Hidden Text
39 suspect characters on 2 pages
Text is altered to blend into the white background of the document.

Our system's algorithms look deeply at a document for any inconsistencies that would set it apart from a normal submission. If we notice something strange, we flag it for you to review.

A Flag is not necessarily an indicator of a problem. However, we'd recommend you focus your attention there for further review.

Dr. Deshraj Meena

(Supervisor)

Match Groups

- 35 Not Cited or Quoted 8%
  Matches with neither in-text citation nor quotation marks
- 0 Missing Quotations 0%
  Matches that are still very similar to source material
- 0 Missing Citation 0%
  Matches that have quotation marks, but no in-text citation
- 0 Cited and Quoted 0%
  Matches with in-text citation present, but no quotation marks

Top Sources

6% Internet sources
2% Publications
5% Submitted works (Student Papers)

Top Sources

The sources with the highest number of matches within the submission. Overlapping sources will not be displayed.

1	Submitted works	National University of Singapore on 2025-04-18	<1%
2	Internet	www.mdpi.com	<1%
3	Internet	baadalsg.inflibnet.ac.in	<1%
4	Internet	hi.tamu.edu	<1%
5	Internet	oro.open.ac.uk	<1%
6	Internet	www.researchsquare.com	<1%
7	Internet	www.rsc.org	<1%
8	Submitted works	Morningside College on 2009-01-28	<1%
9	Submitted works	University of Hull on 2015-05-15	<1%
10	Submitted works	University of Alabama, Huntsville on 2025-03-17	<1%

11	Publication	
Nghe My Tran, Qui Thanh Hoai Ta, Jin-Seo Noh. "Unusual Synthesis of Safflower-S...		<1%
12	Submitted works	
Universiti Teknologi Malaysia on 2021-09-03		<1%
13	Internet	
arxiv.org		<1%
14	Internet	
ijsret.com		<1%
15	Internet	
mjfas.utm.my		<1%
16	Submitted works	
Australian National University on 2022-05-10		<1%
17	Internet	
essay.utwente.nl		<1%
18	Submitted works	
Universiti Teknologi Malaysia on 2022-04-16		<1%
19	Submitted works	
Universiti Putra Malaysia on 2016-12-05		<1%
20	Submitted works	
University of Limerick on 2025-04-10		<1%
21	Publication	
Xiaolong Lu, Zhiwei Xu, Yi Shi, Qi Wang, Jialu Jia, Nan Sun, Bijun Fang, Ningyi Yua...		<1%
22	Internet	
docshare.tips		<1%
23	Internet	
ebin.pub		<1%
24	Internet	
file.scirp.org		<1%

25	Internet	
link.springer.com		<1%
26	Internet	
www.nature.com		<1%
27	Publication	
N. Murugan, R. Jerome, M. Preethika, Anandhakumar Sundaramurthy, Ashok K. S...		<1%
28	Submitted works	
University College London on 2023-03-05		<1%
29	Submitted works	
University of Leicester on 2025-05-17		<1%